Sedimentary Geology xxx (2012) xxx–xxx

Contents lists available at SciVerse ScienceDirect

Sedimentary Geology

journal homepage: www.elsevier.com/locate/sedgeo

Invited Review

Floods, floodplains, delta plains — A satellite imaging approach

James P.M. Syvitski *, Irina Overeem, G. Robert Brakenridge, Mark Hannon

CSDMS Integration Facility, INSTAAR, U. Colorado, Boulder, CO, USA

ARTICLE INFO

Article history:
Received 4 October 2011
Received in revised form 4 April 2012
Accepted 23 May 2012
Available online xxxx

Editor: G.J. Weltje

Keywords:
River sediments
Remote sensing
River basin depressions
Morphology

ABSTRACT

Thirty-three lowland floodplains and their associated delta plains are characterized with data from three remote sensing systems (AMSR-E, SRTM and MODIS). These data provide new quantitative information to characterize Late Quaternary floodplain landscapes and their penchant for flooding over the last decade. Daily proxy records for discharge since 2002 and for each of the 33 river systems can be derived with novel Advanced Microwave Scanning Radiometer (AMSR-E) methods. A descriptive framework based on analysis of Shuttle Radar Topography Mission (SRTM) data is used to capture the major landscape-scale floodplain elements or zones: 1) container valleys with their long and narrow pathways of largely sediment transit and bypass, 2) floodplain depressions that act as loci for frequent flooding and sediment storage, 3) zones of nodal avulsions common to many continental scale rivers, and often located seaward of container valleys, and 4) coastal floodplains and delta plains that offer both sediment bypass and storage but under the influence of marine processes. The SRTM data allow mapping of smaller-scale architectural elements in unprecedented systematic manner. Floodplain depressions were found to play a major role, which may largely be overlooked in conceptual floodplain models. Lastly, MODIS data (independently and combined with AMSR-E) allows the tracking of flood hydrographs and pathways and sedimentation patterns on a near-daily timescale worldwide. These remote-sensing data show that 85% of the studied major river systems experienced extensive flooding in the last decade. A new quantitative paradigm of floodplain processes, honoring the frequency and extent of floods, can be develop by careful analysis of these new remotely sensed data.

1. Introduction

Geologists have gained insight into the functioning of floodplains from the study of modern rivers and their associated Quaternary deposits (e.g. Schumm and Brakenridge, 1987; Schumm, 1991; Asselman and Middelkoop, 1995; Pizzuto, 1995; Blum and Törnqvist, 2000; Schumm et al., 2002). These insights have allowed for the development of floodplain facies models as an aid to interpret the rock record (Galloway, 1975; Postma, 1990; Galloway and Hobday, 1996; Miall, 1996; Bridge, 2003), and for other more conceptual models on the larger-scale response of floodplains to climate and sea level change (Blum and Törnqvist, 2000; Overeem, 2002; Vandenberghe, 2008).

Conceptual models define 'the floodplain' as the relatively flat area surrounding the active river channel that floods during high discharge events — every year to every few years (Fig. 1). Channel breaches and overflow are caused by: 1) overtopping due to floods, extraordinary tidal fluctuations, and wind-driven waves; or 2) mass failure of levee foundations as aided by subsidence, seepage, erosion, earthquake liquefaction and burrowing animals (Smith and Ward, 1998). The flooding of floodplains defines the complexity of ecosystems and water management, including riparian ecosystem dynamics, agriculture, and fisheries. Floodplain tie-channels link swamps and lakes with a river's water level (Rowland et al., 2009). Floodplain area varies with the height and duration (days to many weeks) of the flood wave, and depends on the surrounding topography in the case of a levee breach. Active floodplain size scales with the recurrence distribution of sometimes overlapping flooded areas — this patchwork of flooded areas becomes a statistical distribution over time with some areas being flooded infrequently even when the flood magnitude is small. Floodplains and their coastal deltas may also flood directly from intense rainfall (e.g. monsoons, tropical cyclones), generating both runoff and standing pools of water on their flat surfaces (Brakenridge et al., 1998; Brakenridge and Nghiem, 2004; Syvitski et al., 2009).

Any conceptual model must account for the dynamic nature of floodplains. Floodplain activity varies across historical and geological time, as influenced by sea level fluctuations, climate, tectonics, and human activity. Holocene floodplains may often be distinguished from their associated Pleistocene floodplain deposits (Blum and Törnqvist, 2000), and even deposits representing smaller climatic chronozones can often be distinguishable (Erkens, 2009; Hijma, 2009).

Rivers avulse across wide floodplains: 700 km wide in the case of the Holocene Yellow River. Historical maps help locate these paleo courses: over the last 4000 y for the Yellow River (Fig. 5L), 2000 y for the Nile (Fig. 5D), 1000 y for the Po (Fig. 5U), and the last 200 to 500 y for many other world rivers (Syvitski et al., 2009). Channel avulsions on floodplains and delta plains (e.g. Figs. 8 and 9) are still hotly debated (as summarized in Slingerland and Smith, 2004), with studies documenting the influence

* Corresponding author.
E-mail address: James.syvitski@colorado.edu (J.P.M. Syvitski)

0037-0738/$ – see front matter © 2012 Elsevier B.V. All rights reserved.
doi:10.1016/j.sedgeo.2012.05.014

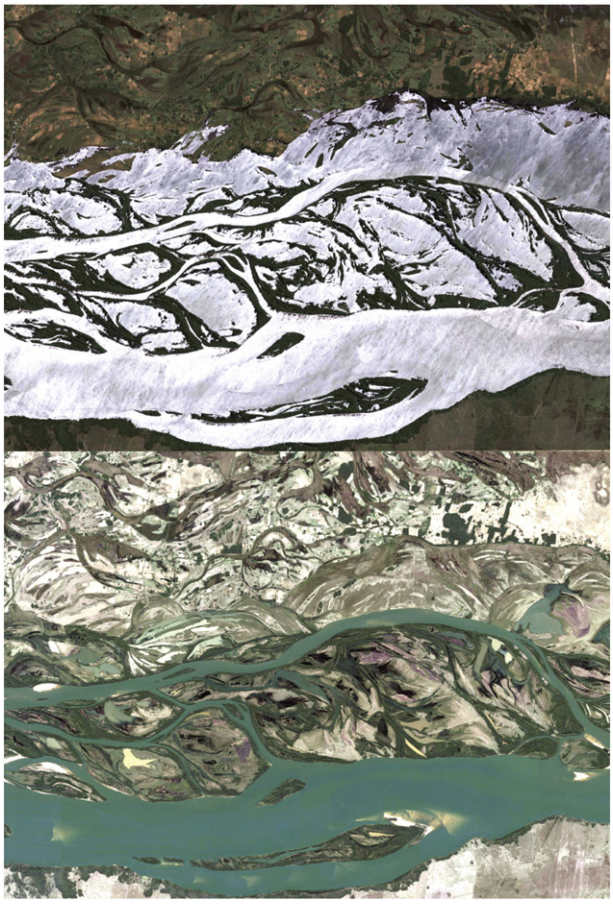

Fig. 1. Parana River orbital images taken at the border between Argentina and Paraguay, SE of the town of Pilar (width of each image is ~10 km). Upper Panel: High discharge, Oct. 22, 2009 ©GeoEye. Lower panel: low discharge, Sept 25, 2005 ©Digital Globe. The low discharge image illustrates the patchwork of amalgamated bars, suggesting continuous evolution; however, most of the bars are completely inundated at high water. Abandoned meandering channels just outside of the flood margin suggest even larger floods occur occasionally.

of human activity (Syvitski et al., 2005), tectonics, earthquakes (Bilham et al., 2007; Bilham and Lodi, 2010) and gradient capture (Stouthamer and Berendsen, 2007; Edmonds et al., 2009; Hood, 2010). From a geological perspective, floodplains encompass the entirety of these interleaved and overlapping floodplains deposits (Bridge, 2003).

Worldwide mapping of floodplain landscape elements and dynamics is now possible using high-resolution remote sensing data (e.g. LANDSAT, SRTM for morphology and MODIS for changes in water levels and sediment loads: Fig. 2). Morphological data allow distinction between bars, levees, splay deposits, and the more featureless flood-cover zones (Figs. 3 and 4). Some floodplain features are not necessarily tied to overbank flooding (Fenneman, 1906), but rather involve the reworking of sediment via within — channel dynamics at high flows, e.g. pointbars or river braids.

The question we pose is: *Do our conceptual models of floodplain processes and landscape development change in the era of global coverage of high-resolution remote-sensing data*? To explore this issue, we survey a selection of global floodplains using consistent orbital imagery and techniques to bridge the gap between modern process understanding and the interpretation of geological deposits. We limit findings to 33 medium- to large-scale floodplains restricted to areas between sea level and the 100 m elevation contour. These are the same river systems used in the recent analysis on global deltas (Syvitski et al., 2009). Even with this limitation, large terrestrial areas of the world are surveyed, as trunk-rivers can sometimes extend 1000's km inland from their river mouth position (Table 1). We concentrate on the surface morphology only of the active floodplains as imaged by the SRTM (Shuttle Radar Topography Mission) interferometric synthetic aperture radar (InSAR). We examine the propensity of these floodplains to flood, based on MODIS (Moderate-resolution Imaging Spectroradiometer) imagery acquired twice daily since 2000, and NASA/JAXA's Advanced Microwave Scanning Radiometer (AMSR-E) imagery acquired daily since mid-2002. Satellite tools such as MODIS and AMSR-E allow near-daily mapping of global rivers at peak flow and the associated flood areas and recurrences.

An important geological cautionary note is that these data are from the Anthropocene — the time when the human species have a major impact on the Earth's surface (see Crutzen and Stoermer, 2000; Zalasiewicz et al., 2008). Most studies that employ modern observations as an aid to interpreting the geological record are subject to this caveat. Although physics remain physics, humans have intervened against the force of gravity, decelerated and accelerated natural processes, focused energy, altered or destroyed ecosystems, and altered the earth's climatology. Using the present as a key to the past must proceed with this knowledge.

2. Methods

Floodplain topography is mapped with the global SRTM survey of February 2000, where an 11-day NASA/NGA Mission obtained a near

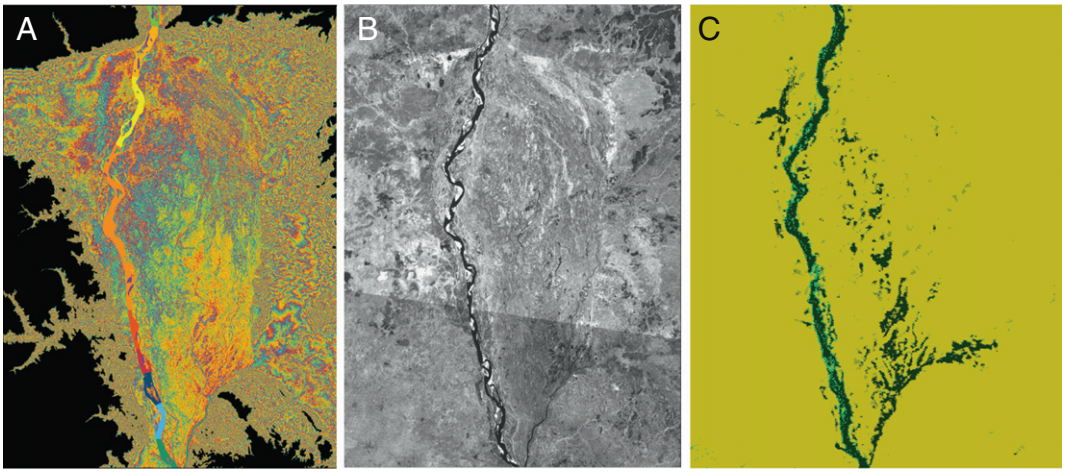

Fig. 2. Floodplain of the Niger River, near the town of Ajaokuta, Nigeria. The width of each image is ~100 km. A: 30 m pixel SRTM C-band InSAR model of elevation (Feb. 2000) — colors change every 1 m of vertical elevation, and cycle every 10 m; black elevations are > 100 m. The river enters the top of the image at 25 m elevation above sea level and exits at 18 m asl. B: 30 m near-infrared LANDSAT image (day 109, 2001) taken at very low discharge. C: MODIS near-infrared 500 m pixel resolution imaging of the Niger R. during flood (day 288, 2006). Black represents clean water pooling from rainfall — greenish black represents river water with higher concentrations of suspended sediment.

Please cite this article as: Syvitski, J.P.M., et al., Floods, floodplains, delta plains — A satellite imaging approach, Sediment. Geol. (2012), doi:10.1016/j.sedgeo.2012.05.014

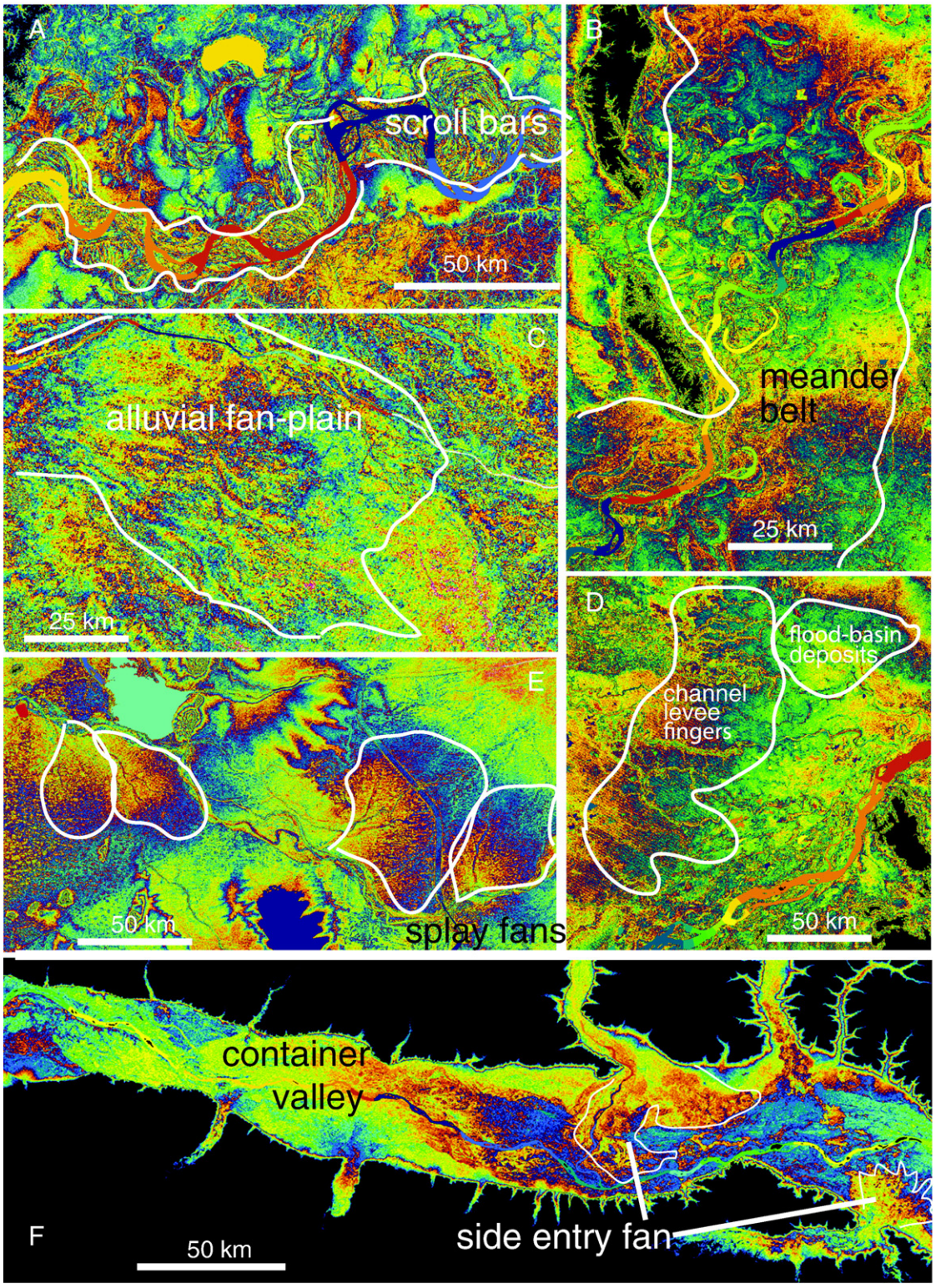

Fig. 3. Architecture elements of floodplain imaged with SRTM C-band InSAR — colors change every 1 m of vertical elevation and cycle every 10 m; black elevations are > 100 m. A) Migrating point bars or scroll bars, Amazon R. B) Meander belt, Mississippi R. C) Alluvial fan plain, Tone R. (Japan), D) Channel levee fingers and flood basin (cover) deposits, Orinoco R., E) Crevasse splay fans off of older (c. 1800's) Yellow R. F) Container valley floodplain with side entry fans, Niger R.

complete InSAR coverage between 60°N and 59°S (Farr et al., 2007). The vertical precision of the SRTM C-band data depends on location, terrain characteristics and surface feature, and has a relative global accuracy of ≈3.7 m (Berry et al., 2007); the world's flatter floodplain areas have surface features with a vertical root mean square error between 1.1 and 1.6 m (Schumann et al., 2008). The horizontal pixel is 1-arc or 3-arc seconds, depending on data processing and data access-restrictions. An SRTM DEM consists of the static heights over land, with tidal areas adjusted to mean sea level with TOPEX/Poseidon-derived ocean heights (Farr et al., 2007). The SRTM Water Body Data sets ocean elevation to

Please cite this article as: Syvitski, J.P.M., et al., Floods, floodplains, delta plains — A satellite imaging approach, Sediment. Geol. (2012), doi:10.1016/j.sedgeo.2012.05.014

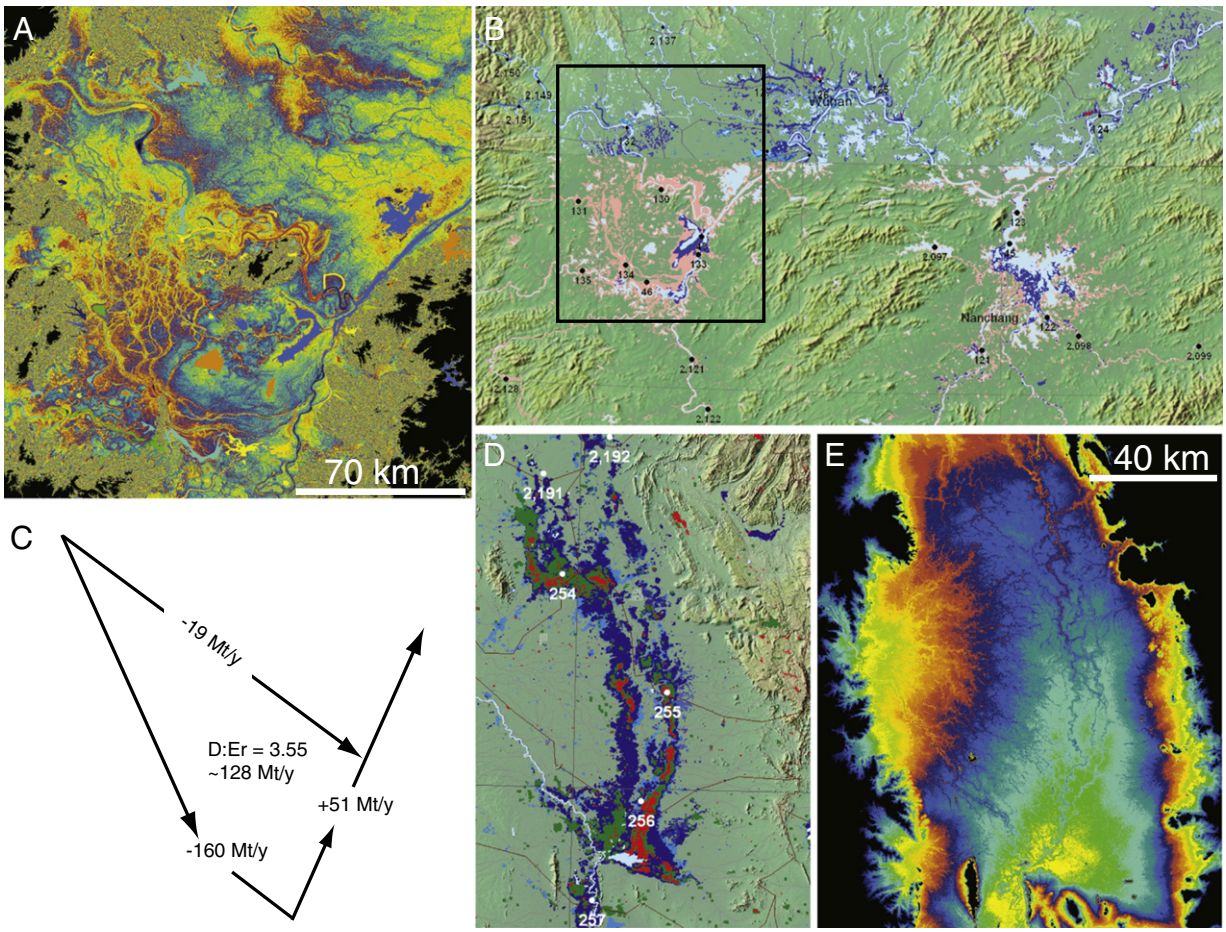

Fig. 4. Examples of floodplain depressions. A) Dong Ting depression located at the intersection of the Yangtze and Xiangjiang Rivers (China): imaged with SRTM C-band InSAR — colors change every 1 m of vertical elevation, black elevations are >100 m. B) 2000 to 2010 flooded areas (colored in blues and pink) along the lower Yangtze, showing the location of the A) with the black box. Also shown further to the right is the Poyang Lake depression area (cf. 6C). C) Mass balance of the sediment flux across the Dong Ting depression shown in A) (after Chen et al., 2010). Over a 50 year period prior to the Three Gorges Dam, the depression stored 128 Mt/y. D) 2000 to 2010 flooded areas (colored in blues and pink) along the lower Chao Phraya (Yom & Nam R.) flowing into the Phichit tectonic depression, Thailand. E) SRTM topography of the Phichit depression — note western (Ping) side entry fan.

0 m; lakes >600 m in length are brought to a constant height, and rivers that exceeded 183 m in width are monotonically stepped down in height (Farr et al., 2007). Our SRTM images (Figs. 2A, 3, 4A, E, 6, 8) employ color changes every 1 m of vertical elevation, with colors cycled every 10 m. Striping and vegetation canopy removal can further refine SRTM data (Gallant and Read, 2009), but has not been employed here. The study was limited to floodplain topography seaward of the 100 m in order to ensure that we did not approach the pixel resolution limitations of the SRTM data (90 m in many cases). Architectural elements were identified from SRTM as well as by using much higher resolution sensors (ASTER, Landsat, SPOT, GeoEye)

Flood mapping is based on twice daily, wide-swath space-borne optical sensors, operating at a spatial resolution of 250 m. A automated processing algorithm for the MODIS band 1 and 2 data from instruments aboard NASA's Terra and Aqua spacecraft is available from 2000, and provides near-real time measurements of floodplain inundation (Brakenridge and Anderson, 2006). The present algorithm ingests four images (Terra and Aqua, each day, for two days). A cloud shadow filter removes this source of error (shadow can otherwise be misclassified as water) and a filling process takes advantage of moving cloud obscuration to increase spatial coverage. During flood events (Fig. 2C), the evolving flood wave can be followed, or the data can be aggregated to provide total inundation for the flood event (Fig. 9).

Satellite river discharge sensing is a useful complement to flood mapping, as it provides a numerical estimate of the water flux along a river reach at all times. In this regard, NASA/JAXA's AMSR-E mission provides the capability to measure changing river dynamics from orbit, from mid-2002 to the present (Brakenridge et al., 2007). AMSR-E data on floods is presently operational as the "Global Flood Detection System" (GFDS) portion of the European Commission-supported "Global Disaster Alert and Dissemination System" (GDACS) (DeGroeve et al., 2007), and as the Dartmouth Flood Observatory "River Watch", a global river discharge and runoff measurement system (Brakenridge, 2010). As rivers rise over a 5 km measurement reach, surface water areal extent within the defined area increases monotonically (Figs. 1 and 10), and this wide-area, frequent-repeat sensor can detect and consistently measure this change. AMSR-E provides near-daily coverage for most of Earth's land area and with minimal interference from cloud cover. The technique is based on the exceptional sensitivity of the microwave AMSR-E band at 36.5 GHz, descending orbit, horizontal polarization, to surface water and it uses real time swath data. The discharge estimator is a ratio of calibration-target radiance (expressed as brightness temperature), for a local land parcel unaffected by the river, to measurement-target brightness temperature, for a pixel centered over the river (Fig. 10).

As so obtained and calculated, the microwave signal ratio is a discharge proxy (as is ground-measured stage): both must be calibrated to discharge units via rating curves (Bjerklie et al., 2003). We have tested the sensitivity and accuracy of the orbital measurements along U.S. rivers using data from situ gauging stations, with favorable results (Brakenridge et al., 2007). Measurement locations are chosen to maximize measurement sensitivity and reliability (Fig. 10). Even when extensive artificial levees are present, most rivers include reaches where water area responds

Please cite this article as: Syvitski, J.P.M., et al., Floods, floodplains, delta plains — A satellite imaging approach, Sediment. Geol. (2012), doi:10.1016/j.sedgeo.2012.05.014

to discharge changes, such as tributary stream junctions, slip-off slopes across the inside bends of meandering rivers, channel bars and islands, and other features (Brakenridge et al., 1998). As discharge increases and rivers rise, river reach total water surface area also increases, and orbital remote sensing can detect and quantify the change.

3. Landscape-scale floodplain zones

Each of the 33 lowland floodplains surveyed was described for their overarching patterns of large-scale landscape elements (Figs. 3, 4, 5, Table 1). The rivers reached their 100 m-elevation above sea level (a.s.l.) on average 1100 km in upstream distance from the coast as measured along their thalweg. Four large landscape-scale elements are recognized: container valleys, floodplain depressions, nodal avulsion zones and coastal deltas. Arbitrary assemblages of these landscape elements were able to capture all of the varietal floodplains investigated.

3.1. Container valleys

Within the ≤100 m asl topographic study limits, only 12% of the floodplains surveyed offered no container valleys (e.g. Yellow, Indus, Irrawaddy, Tigris-Euphrates, and the Ganges Rivers) — their container valleys being located at higher elevations. Container valleys are long relatively narrow parts of the river system that function as conveyor belts of highland sediment delivery to the lowland floodplains. Significant lengths of container valleys may be locally expressed as gorges (Mahakam, Yangtze, Danube, Congo, Limpopo, Mahanadi, Brahmani, Krishna, Godavari, Sao Francisco and Pearl Rivers), where the river channel occupies the entire narrow valley and is floored with exposed or thinly mantled bedrock. The valley operates as a sediment transit zone, or even sediment production if the gorge is undergoing ambient uplift. Most container valleys are, however, filled with enough sedimentary deposits so that the valley floor has aggraded to become 5 to 10+ times wider than the river channel width (e.g. Fig. 3f). Some container valleys may contain fluvial terraces (e.g. Amazon, Mississippi, Parana, Vistula, Volga Rivers) offering evidence of alternation between periods of erosion and aggradation. Over time spans of decades to centuries and longer, the river channel sweeps across the container valley, simultaneously eroding and depositing both channel and floodplain sediment. Often the river location is influenced by the valley margins, where the river channel "locates" for longer distances than at more valley-interior locations. The impact of side entry tributaries is particularly strong within container valleys, as their tributary delta/fan systems are magnified within the container valley (e.g. Fig. 3f). Container valleys offer limited width, and thus flood waves as mapped from MODIS often extend to the walls of the container valley. Changes in the width of a container valley lead to small changes in downstream valley slopes out of equilibrium with the normal down-valley exponential decrease in slopes (e.g. Fig. 7).

3.2. Floodplain depressions

Fifty-five percent of the floodplains contained depression zones at elevations <100 m asl (Table 1). These depressions have many origins: foreland basins (peripheral, retroarc) including foredeep and backbulge; graben, half-graben and other fault complexes; dynamic topography supported by mantle flow; lithospheric cooling following stretching; other isostatic and flexural depressions; and salt or mud tectonics. The depressions are characterized as including some of the following identifiers: statistically flatter down-valley slopes (Fig. 7); greatly expanded widths compared to the container valley widths (Fig. 5); multiple secondary or overflow river channels similar in nature to deltaic distributary channels (e.g. Figs. 2 and 4A); regional zones of swamps and lakes connected to the main river channel (Figs. 4B, E, 6C, D, G, H). None of these features alone is diagnostic. For example there are many other types of floodplain lakes — e.g. cutoff oxbow lakes (Fig. 6A), scroll-bar lakes (Fig. 6B), compaction lakes (Fig. 6C), and thermokarst or thaw lakes (Fig. 6F). Floodplain depression zones are highly prone to flooding, often annually (Fig. 4B, D).

Flow divergence through multiple channels or lakes point to these floodplain sectors as locations of significant sediment sequestration. Storage in sediment routing system has the important effect of buffering sediment discharge signals, and statistically lengthens transit times of sediment mass being moved seaward. Satellite imagery shows depression lakes with bright reflectance as a result of high sediment concentrations as the seasonal flood wave pushes sediment-laden water across the zone of depression (Kettner et al., 2010). The fact that these river-connected lakes may exist over millennia suggests that the rate of subsidence is greater than the rate of aggradation. Some examples are illustrative of the variety of depression zones:

1) The Mompox depression located upstream of the Magdalena Delta (Fig. 7) is covered with hundreds of lakes (Fig. 6D). Seasonal overflow and levee failures along the Magdalena cause extensive flooding (April–Nov.). Over the last 7500 y, the Mompox depression has experienced an area-averaged aggradation rate of 3–4 mm/y, with deposit thicknesses ranging from 10 m to 130 m thick (Kettner et al., 2010). Based on 27 y of measurements, 14% of the Magdalena load is sequestered within the depression (Kettner et al., 2010). Clearly these rates are not geologically sustainable, but they do provide an indication of the trapping potential of floodplain depressions.
2) The Poyang depression has a surface expression as an inland delta feeding Lake Poyang (Fig. 6C). The lake sequesters much of the annual sediment load of the Gan and Xiu Rivers before its drainage into the main stem Yangtze River (Fig. 4B illustrates the recurring floods in this depression). Lake levels drop quite low on an annual basis during the dry season.
3) Perhaps the best-studied depression is the Dong Ting located at the intersection of the Yangtze and Xiangjiang Rivers (China). Over the later half of the 20th century, the depression sequestered 128 Mt/y, largely through overflow channels that drain into Dong Ting Lake (Fig. 4A) with only a minor contribution attributed to aggradation of the main Yangtze River channel (Fig. 4C) (Chen et al., 2010). Human control of the discharge volume of the overflow channels for purposes of agriculture is thought to have accelerated the rapid fill of Dong Ting Lake (Chen et al., 2010). Much of the sediment sequestration takes place during the monsoon season (June–Sept), with the arrival of the summer flood wave, and when much of the depression surface is temporarily under water (Fig. 4B). During the rest of the year, the depression zone is a net supplier of sediment (Fig. 4C, Chen et al., 2010).

3.3. Zones of nodal avulsions

Some river systems offer extraordinary wide floodplains (river channel width to floodplain width >1:500) over which the main river channel is episodically re-located through nodal avulsions at time scales of centuries to millennia, e.g. Yellow, Tigris-Euphrates, Indus (Fig. 9), and Brahmaputra (Figs. 8B and 10). The result is a distinctive fan shape to the topographic contours wherein paleo crevasse splay fingers separate from the paleo channel locations (Fig. 8B). For some rivers, these patterns associated with nodal avulsions are limited to the delta complex only, e.g. Irrawaddy (Fig. 8A), Mississippi, Mahanadi, Krishna, Brahmani, and Godavari.

A major avulsion may take decades to be completed. A major avulsion of the Brahmaputra River to eventually occupy the Lobnee River [renamed as the Jamuna River] in the late 1850's required more than 25 years to complete. Similarly the Yellow River flowed simultaneously for many decades into both the Yellow Sea and the Bohai Sea, according to maps published in 1389 (Da Ming Hun Yi Tu). There are justifications for this slow process. Firstly, an avulsing river needs to incise significantly into a floodplain in order to carve a stable channel capable of

Please cite this article as: Syvitski, J.P.M., et al., Floods, floodplains, delta plains — A satellite imaging approach, Sediment. Geol. (2012), doi:10.1016/j.sedgeo.2012.05.014

Table 1
Selected floodplains described up to 100 m above sea level.

River, country	Length km to 100 masl	Floodplain:delta plain area	Element description	Floodplain depression	Climate zone	Abundance of lakes	Flooding characteristic
Amazon, Brazil	4100	8:1	Architecture varies for each of the mostly sinuous tributaries. Trunk channel results in mega-scale scroll-bar topography. Amazon > 50 km wide in wet season.	Above 100 m elevations	Equatorial – tropical	Very high	Extensive wetlands floods annually.
Amur, Russia	1884	50:1	Very wide floodplain. Braided over the largest scale, meandering channels with prominent scroll bars.	1) Swamps SW of Chabarovsk; 2) Swamps W of Harbin	Subarctic – monsoon	Many thaw lakes & large marsh lakes with tie-channels	Ice break-up flooding, vast monsoonal flooding.
Chao Phraya, Thailand	730	2.5:1	Floodplain progrades onto delta plain with levees and crevasse splays. Tributary fans prograde onto floodplain from valley sides. High sinuosity stretch in tectonic depression.	Phichit basin	Tropical	Minor, oxbow lakes, Bung Boraphet	Very widespread.
Congo, Zaire	198	N/A as FA >>100 m	Narrow channel, structurally controlled channel meanders	Above 100 m elevations	Equatorial -tropical	Above 100 m elevations	Few localized floods
Danube, Romania	1826	13:1	Large active floodplain separated by narrow stretch through Carpathians. Straight channel, human-controlled with dikes	Several	Temperate	Yes, particularly on the delta	Moderately widespread
Euphrates-Tigris, Iraq	1170	20:1	Wide floodplain, high sinuosity	Unknown	Arid	Few, isolated lakes	Localized flooding occurs frequently
Fly, Papua New Guinea	902	4:1	High sinuosity 2–3, except in tidal river. Many abandoned channels with large-scroll-bar topography	Large depression at convergence of Strickland-Fly	Tropical	Very abundant lakes with tie-channels and wetlands	Frequent rain-induced flooding
Ganges-Brahmaputra, Bangladesh	1365; 1100	4:1	Ganges dominated by meandering, Brahmaputra as braids. Many crevasse splays. Many tidal channels in delta	Kalni Basin (floods annually)	Monsoon	Yes	Annual flooding extends to Himalayas
Godavari-Krishna, India	513; 316	1:20	No floodplain, just delta plain. River is sandy and braided.	No	Monsoon	Few, on the delta	Annually
Indus, Pakistan	1188	8:1	Large meandering, sinuosity 1.2–1.7 sandy-bed, active migration.	Near delta, frequent earthquakes	Arid-monsoon – snow fed	Few, on the delta	Every 3 yrs
Irrawaddy, Burma	1078	1:20	Floodplain restricted by highlands, mostly sandy & braided channel style; large delta.	No	Monsoon	Few	Widespread with cyclonic flooding
Limpopo, Mozambique	361	8:1	Meandering channel in sandy-bed	Chokwe-Chibuto depression	Tropical	Many lakes with tie-channels	Cyclonic flooding
Mahanadi-Brahmani, India	324	1:30	Hardly any floodplain, braided with 2 km wide floodplain, relatively sandy, main channel belt sinuosity 1–1.3	No	Monsoon	Few, on the delta	Abundant monsoonal flooding, widespread in delta

Please cite this article as: Syvitski, J.P.M., et al., Floods, floodplains, delta plains — A satellite imaging approach, Sediment. Geol. (2012), doi:10.1016/j.sedgeo.2012.05.014

Mahakam, Indonesia	591	5:1	Highly meandering, highly vegetated	Mahakam intermontane depression	Tropical	Large lakes with tie-channels, some oxbows	ENSO impact
Magdalena	760	5:1	Highly meandering, sinuosity of 1.1–1.4, relatively straight channel in steeper parts of profile	Mompox depression	Tropical	Many lakes in tectonic depression.	Small, frequent floods in existing extensive wetlands
Mississippi	1451	8:1	Prominent meandering (up to local stretches with sinuosity of 2.5) Large scroll-bar geometry	No	Temperate, subtropical	Abundant oxbow lakes	Frequent in main channel belt and delta tributaries
Mekong	1009	1:15	Large crevasse splays restricted to delta	Yes, back filling of Tonle Sap	Tropical-monsoonal	Large depression lake	Frequent flooding
Niger, Nigeria	880	1:3	Channel sinuosity varies 1–1.2, stretches of 1.7 in growth fault bounded sub-basins near delta apex.	Illushi basin???	Tropical	Many old oxbow lakes, rapidly vegetated	Frequent flooding
Nile, Egypt	1240	10:1	Narrow container valley, relatively straight channel	Back filling of Birkat Qaran	Arid	Depression lake	Controlled
Orinoco, Venezuela	1570	1:1	Relatively straight channel belt, large-scale abandoned scroll bars	Caprota swamps	Tropical	Abundant, related to old point bars, wetland & swamps	Widespread in floodplain, less in delta region
Parana, Argentina	1888	10:1	Many scroll bars, multiple channels with medium-high sinuosity	Part of the Grand Chaco	Tropical	Abundant, related to wetland and swamp areas	Annually widespread through floodplain
Pearl, China	1145	1:40	Multiple channels, small mid-channel bars, floodplain restricted by highlands	No	Tropical	None	Localized floods and more abundant in the delta
Po, Italy	467	20:1	Narrow channel, abundant avulsions in larger floodplain, small sandy bars	Suzzara sag	Temperate – Mediterranean	Few	Local flooding from rain on snow events in higher basin
Sao Francisco, Brazil	226	1:10	Low sinuosity due to small container valley, sandy mid-channel bars	Above 100 m elevation	Subtropical	Abundant oxbow lakes and floodplain back-swamps	Occasional
Tone, Japan	227	20:1	Relatively straight channel course with sandbars, until small deltas with tidal impact	No	Monsoon – snow fed	Few	Low flood frequency, heavily engineered
Vistula, Poland	548	2:1	Low sinuosity, single channel	No	Temperate	Few	Local spring flooding, mostly embanked
Volga, Russia	2800	2:1 Holocene floodplain	Large scroll-bar remnants, meandering channel, sinuosity 1.1–1.3. Large vegetated mid-channel bars	Part of Russian Platform down warping	Semi-arid	Many, Baer hills and lakes	Very frequent, widespread spring floods and rain-induced floods
Yangtze, China	1771	1:5	Relatively straight	Several, e.g. Poyang, Dong TIng	Several climate zones	Linear-shaped lakes from abandoned channels	Frequent and widespread
Yellow, China	750	1:20	Meandering, sinuosity between 1.1 and 1.5. Abandoned Holocene super-elevated channel belts Many crevasse splays	Several, e.g. Hongze Lake, Nanyang Lake	Several climate zones	Few	Frequent and widespread (less so with dams)

Please cite this article as: Syvitski, J.P.M., et al., Floods, floodplains, delta plains — A satellite imaging approach, Sediment. Geol. (2012), doi:10.1016/j.sedgeo.2012.05.014

carrying the river's discharge during flood. Large rivers have channel depths of 10's of meters. The Amazon has channel depths of 50 to 100 m over a 2000 km distance inland of the coast (Filizola et al., 2002). When a river breaches its levee, the floodplain floor is just a few meters below the top of a levee. The volume required to contain a major river, and thus the amount of sediment necessary to be carved out from the floodplain, depends on its discharge characteristics and the length of the new reach. In the Brahmaputra case, the new Jamuna reach was 150 km long. Thus the sediment volume related to the incision into the floodplain would be, roughly, 4.5 Gt. If we assume that the river's discharge could only increase its existing transport capacity by some small percentage say 25%, to allow new channel erosion, then the river avulsion would require approximately 20 years to complete, similar to the observed avulsion duration. More sudden avulsions do occur, particularly when the water depths required to carry the discharge are available through existing paleo channel belts.

3.4. Coastal lowlands and delta plains

Most of the investigated rivers have a delta expression — a lobate sedimentary deposit that in plan view protrudes into the coastal ocean, out from the ambient coastline, but narrows inland, towards the feeder river. Delta systems are in part bypass systems, where only a portion of the sediment that travels down the river is retained (Overeem et al., 2005). The formation of a delta reflects the magnitude of sediment supply, available accommodation space, and fluvial, coastal and marine dispersal energy (Syvitski et al., 2005; Syvitski, 2006). Coastal deltas are dominated by flow divergence — channels split into distributaries, sometimes with downstream rejoins, and where the influences of transverse pressure gradients and momentum are most important (e.g. Fig. 5D, Q, R, S, O, T, C3). The Congo River in contrast exemplifies a bayhead delta (Fig. 5I) wherein a continental slope canyon penetrates into the bay — delta sediment is thus shed directly into the deep ocean bypassing the continental

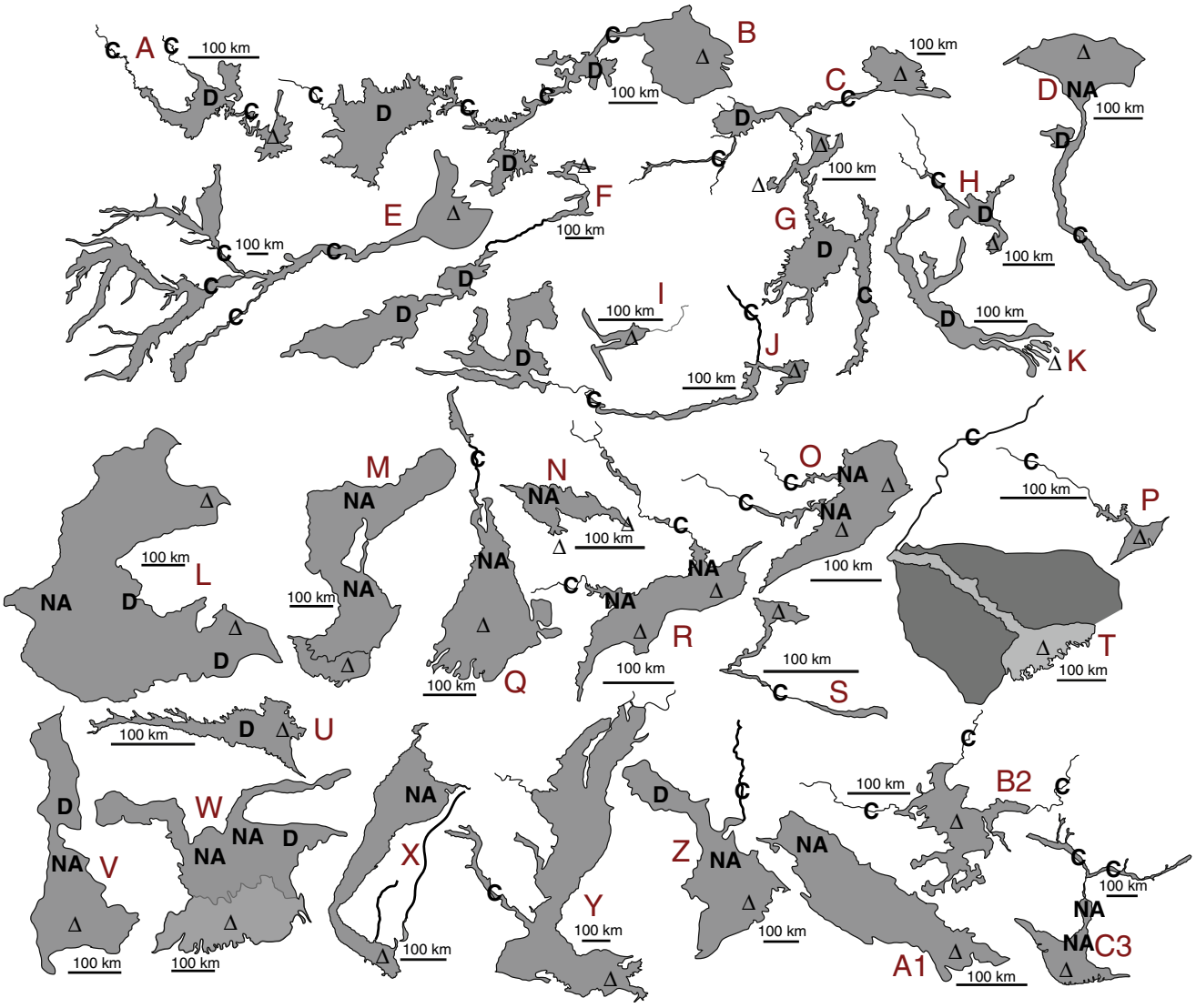

Fig. 5. Shown is the outline of 29 Holocene-active floodplains and their delta plains, to a height of 100 m above sea level (except where noted). Many of the rivers also support higher elevation floodplains. The floodplains may enclose higher standing geological islands or Pleistocene terraces of limited size. Floodplains are not drawn to a common scale (shown). Floodplain boundaries are based on tracings from SRTM imaging and as supported by LANDSAT, SPOT, and Digital Globe imagery. Δ represents the approximate center of a delta; D represents the approximate center of the floodplain depression, C is the container valley, and NA is the nodal avulsion location. A) Mahakam (Borneo), B) Yangtze (China), C) Orinoco (Ven.), D) Nile (Egypt), E) Amazon (Brazil), F) Amur (Russia), G) Magdalena (Columbia), H) Limpopo (Mozambique), I) Congo (Zaire) — note its major floodplain lies above the 100 m study limit, J) Danube (Romania), K) Fly (Papua New Guinea), L) Yellow (Huanghe, China), both its active (upper) and inactive (lower) delta locations shown, M) Indus (Pakistan) showing the tidal flat boundary, N) Tone (Japan) shows both its active (right) and inactive (left) deltas, O) Mahanadi and Brahmani (India), P) Sao Francisco (Brazil), Q) Irrawaddy (Burma), R) Krishna and Godhavari (India), S) Vistula (Poland), T) Volga (Russia) only drawn to 10 m asl, showing both the Holocene system (light gray) and the Pleistocene system (dark gray), U) Po (Italy), V) Chao Phraya (Thailand), W) Ganges (India) and Brahmaputra (Bangladesh, India) showing the extent of its delta, X) Parana (Argentina) system, Y) Mississippi (USA), Z) Mekong (Vietnam), A1) Tigris & Euphrates (Iraq), B2) Pearl (China), and C3) Niger (Nigeria).

Please cite this article as: Syvitski, J.P.M., et al., Floods, floodplains, delta plains — A satellite imaging approach, Sediment. Geol. (2012), doi:10.1016/j.sedgeo.2012.05.014

shelf. Some of the deltas (Amazon, Fly Fig. 5K) have such strong tidal energy that the lobate shape is replaced by a series of offshore delta islands.

The ratio of the floodplain area (within the ≤100 m a.s.l. limits) to delta plain area (FA:DA Table 1) ranges from 50:1 for the Amur, Russia, to 1: 30 for the Pearl, China. The Amur's excessively small delta is a product of its history: the Pleistocene delta is located ~50 km offshore on Sakhalin Island and is separated by very shallow ocean water from the river mouth due to Holocene sea level rise. Much of the delta plain is thus submerged in 1 to 5 m water depths. On the other extreme, the Pearl River drains high relief topography offering few locations for sediment sequestration within its constrained floodplain: most of the sediment is delivered and deposited at the delta. The Indian deltas (Brahmani, Godavari, Krishna, Mahanadi) similarly serve as their river's main depocenter. In a few cases, the FA:DA ratio is simply influenced by the 100 m elevation limit of the survey (e.g. Sao Francisco, Congo).

Syvitski and Saito (2007) offer a database of 17 environmental descriptors of 51 world deltas, including the number and dimensions of distributary channels, delta dimensions and gradient. The functioning of lakes on deltas is a truly understudied problem, from a "landscape into rock" perspective. Isolation of the river channel from the delta plain by engineering (stop-banks, bunds, or stabilized levees) has recently reduced (e.g. Indus) or eliminated (e.g. Mississippi, Nile) sediment delivery to delta plain lakes. Additionally, many of the delta lakes are artificial (e.g. shrimp ponds of the Chao Phraya, rice paddies of the Mekong).

The down-valley topographic profiles of the main stem channels are well ($R^2 > 0.96$) represented by simple exponential (e.g. Fig. 7: Niger), or 2nd-order polynomial equations (e.g. Fig. 7: Magdalena, Mississippi), or even a complimentary error function. The step-like offsets to these curves are attributable to geological influences including faults and tributary junctions (Fig. 7). Although it remains possible to distinguish the delta form on these profiles, from their extremely low gradient slopes near sea level (e.g. Mississippi, Fig. 7), in some cases a delta's down-slope profile is simply a continuance of the river profile (e.g. Niger, Magdalena, Fig. 7).

4. Floodplain architectural elements

For the continental scale river systems we have studied, SRTM data clearly images smaller-scale architectural elements typical of fluvio-deltaic systems, including active meander or braided river channels and bars, but also older abandoned channels, point bars, scroll bars, oxbow lakes, levees, and crevasse splays (Fig. 3). Side entry fans discharging into container valleys clearly displace the modern channel-belt position (e.g. Fig. 3F). Many different types of lakes are evident (Fig. 6); systematic quantification of their geometries is made possible by using the vector-based SRTM Water Body Data (SWBD). Paleo channels are particularly well imaged with SRTM data in drier regions. Interestingly, abandoned channels may show fluvial patterns different from the modern equivalent, reflecting either different discharge (climate) patterns, or the influence of human channel modifications. The Indus River, for example, had much higher sinuosity (>2.5) before the 19th century compared to the 20th century sinuosity (<1.5) (Fig. 9).

5. Mapping of floods

Until NASA launched flood-mapping capable satellites 10 to 15 years ago, and as augmented by other agencies that deployed orbital sensing

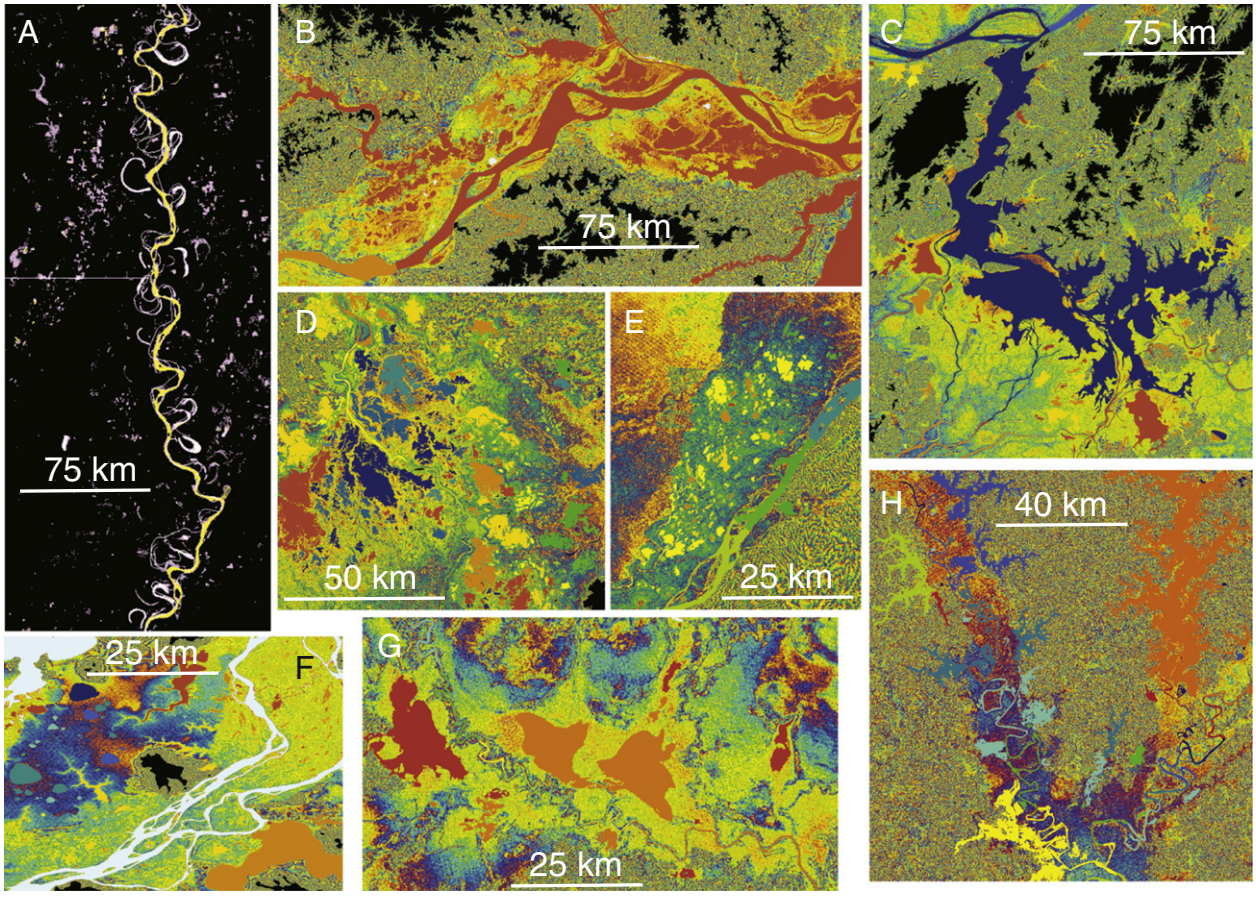

Fig. 6. Floodplain lakes. A) MODIS inverted NIR image of the Mississippi (USA) oxbow lakes. B)-H) SRTM C-band imagery — colors change every 1 m of vertical elevation; black elevations are >100 m. B) Amazon (Brazil) point bar lakes. C) Poyang (tectonic depression) Lake (China) fed by the Gan/Xiu inland river delta with drainage to the Yangtze (top of image). D) The complex lake system of the Mompox depression through which flows the Magdalena River (Columbia), E) Compaction lakes on a portion of the Parana floodplain (Argentina). F) Thermokarst (thaw) lakes within the Amur floodplain (Russia), G) Lakes (e.g. Jempang, Semayang, Melintang) of the Mahakam intermontane depression (Borneo). H) Ria lakes of the Fly River tectonic depression (PNG) located at the junction of the Strickland and Fly Rivers.

Please cite this article as: Syvitski, J.P.M., et al., Floods, floodplains, delta plains — A satellite imaging approach, Sediment. Geol. (2012), doi:10.1016/j.sedgeo.2012.05.014

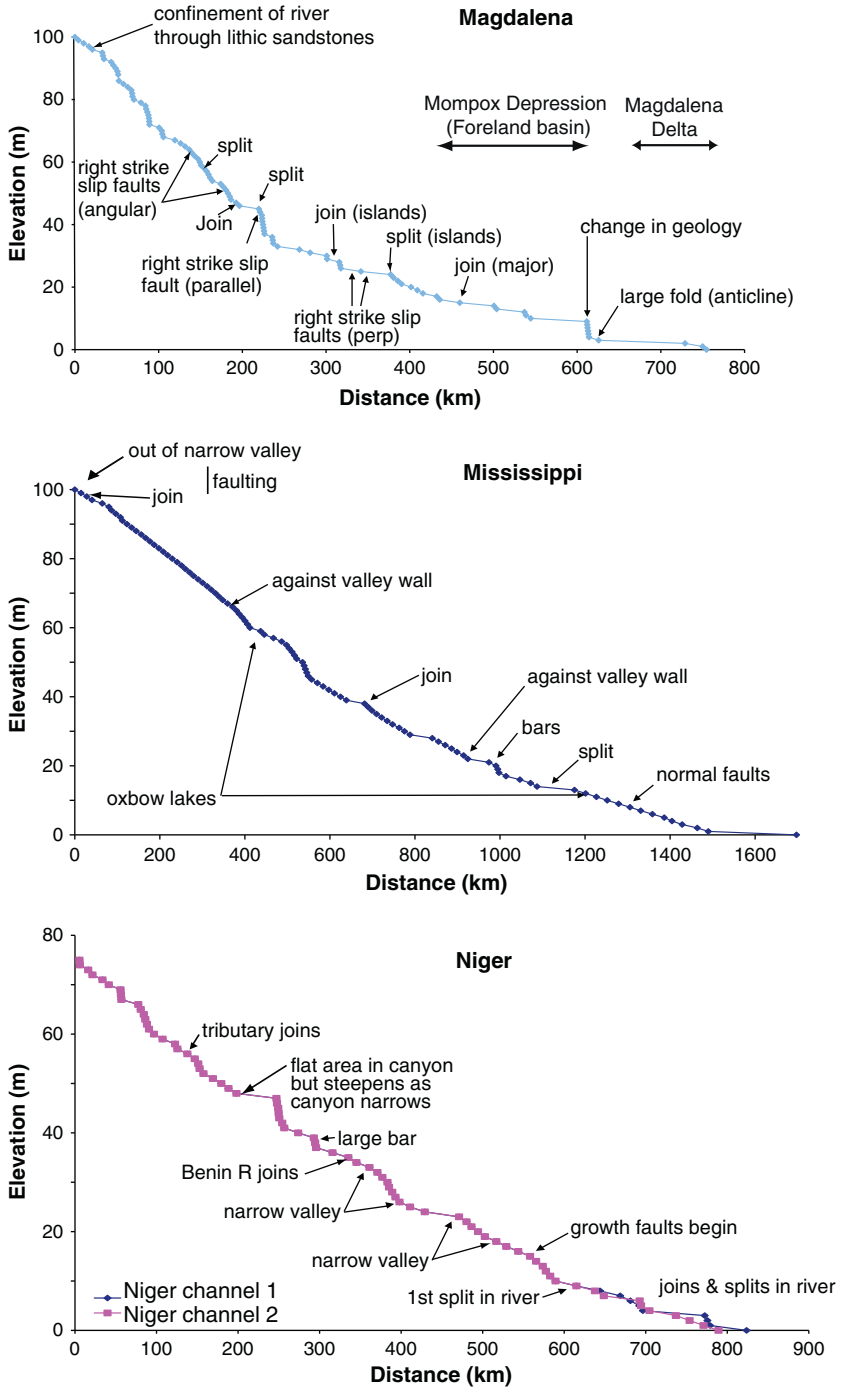

Fig. 7. Thalweg profiles of three representative rivers: Magdalena (Columbia), Mississippi (USA), Niger (Nigeria), as provided in the SWBD/SRTM elevations.

systems, scientists had a limited view of the extent and frequency of flood inundation over the global terrestrial surface. Previous surveying relied principally on case-study information describing a particular event, and was limited to a few well-studied and well-sensed rivers (e.g. Asselman and Middelkoop, 1995; Walling and He, 1997). Here we provide four illustrations of floodwater inundation of lowland floodplains (Figs. 4B, D, 10, 11D) as witnessed from sensors orbiting above. Floodplain depressions are especially vulnerable to flooding, often annually, e.g. the Dong Ting depression (Fig. 4B) or the Sylhet Basin in the Ganges-Brahamaputra fluvio-deltaic system (Fig. 10). Those river systems that have an extremely wide floodplain, such as the Indus show floods mostly near the active channel belt, but with more rare reoccupation of floodwater into paleo channel belts. The source of information employed in constructing the example flood maps and other flood inundation products analyzed for Table 1 is available for review or download at http://floodobservatory.colorado.edu/.

The limitations to the global flood imaging and mapping products include: 1) spatial resolution issues, and 2) temporal duration issues. Considering the global fluvial domain of ~100 Mkm^2 (Syvitski et al., 2005), and the 250 m spatial resolution of MODIS-flood imagery, then 1.6 billion pixels are examined twice daily for global water cover change. Higher resolution imagery (e.g. SAR) covering much smaller spatial domains provides additional detailed information. The temporal duration issues mostly relate to the fact that the satellite systems have been in operation only for a decade (somewhat less in the case of AQUA). Given that the return interval for extreme events can extend over decades to centuries, the MODIS-derived flood inundation mapping is thus very conservative for interpreting the rock record, and possibly misleading.

Please cite this article as: Syvitski, J.P.M., et al., Floods, floodplains, delta plains — A satellite imaging approach, Sediment. Geol. (2012), doi:10.1016/j.sedgeo.2012.05.014

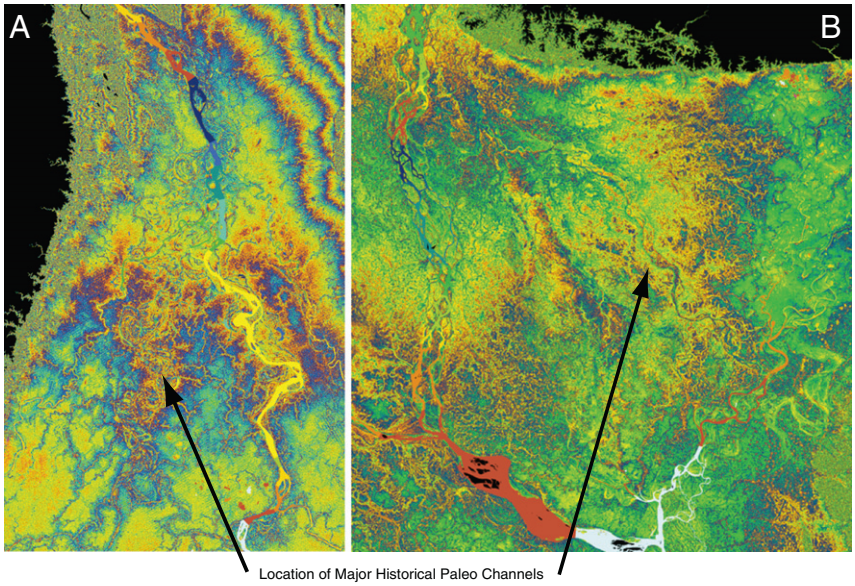

Fig. 8. Floodplains meet delta plains illustrated using SRTM C-band imagery — colors change every 1 m of vertical elevation; black elevations are >100 m. A) Irrawaddy (Burma), B) Brahmaputra (Bangladesh). In both examples there has been a major shift in the main river channel in historical times (Irrawaddy circa 1700's, Brahmaputra 1850's). Both images show sediment levee fingers protruding onto flat delta plain sediments.

Some rivers have experienced a 100 yr or a 500 yr flood in the last decade of mapping, while others have been subjected to only the "~10 yr" event. Each year that passes thus provides increasingly complete evidence into how a floodplain operates under flooding conditions across the earth's surface.

6. Flood discharges

Calculating the discharge magnitude during a significant flood event is a combination of art and science. Whereas maximum discharges have been published for many large rivers (Wohl, 2007), they are considered

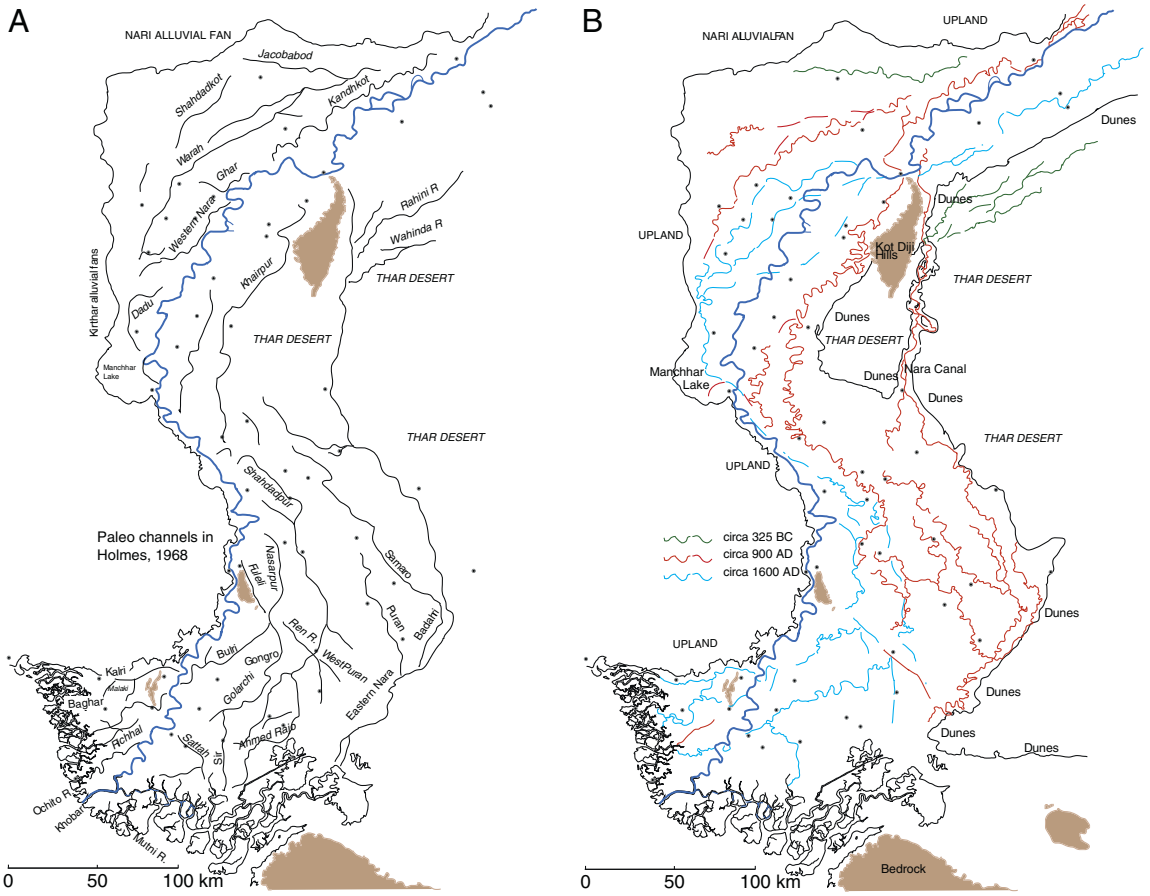

Fig. 9. Comparison of A) Map of the Indus paleo channels from the widely reproduced Holmes (1968) with B) geo-referenced paleo channels identified on SRTM imagery. Both images are of the Sindh province Pakistan, showing the Indus floodplain. Note that the SRTM-identified channels show the sinuosity of the paleo channels compared to the modern Indus (shown in dark blue). Dots are geolocated towns and villages.

Please cite this article as: Syvitski, J.P.M., et al., Floods, floodplains, delta plains — A satellite imaging approach, Sediment. Geol. (2012), doi:10.1016/j.sedgeo.2012.05.014

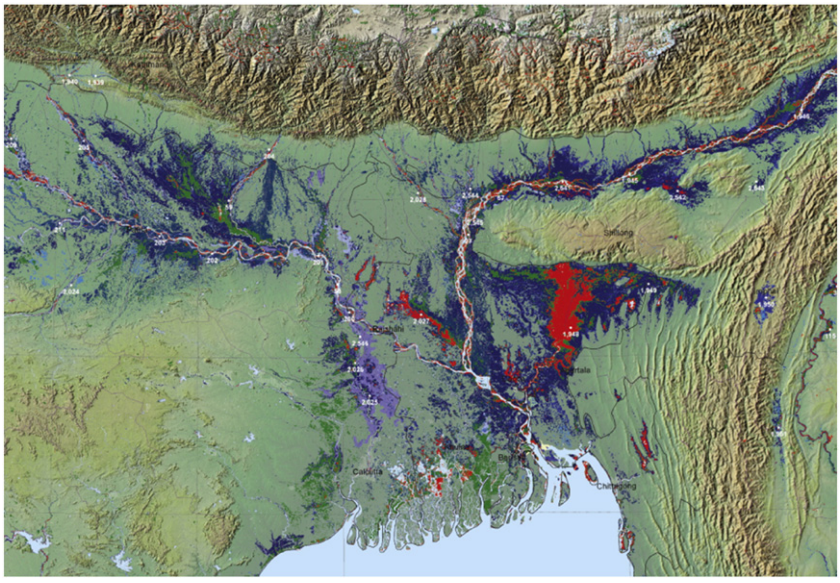

Fig. 10. DFO-produced spatial flood coverage (1999–2009) of the Ganges-Brahmaputra Rivers and joint delta. Colors represent different years with more recent years overlying earlier flooded areas. Often flooded areas reoccur from year to year.

estimates at best. Large floods are rarely directly "measured". Estimated discharge is normally based on existing rating curves for stage height at a measurement station — wherein a survey of low to high discharge events are sampled in terms of 2-dimensional velocity across a well-surveyed cross-section of a river reach. The rating curve allows for changes in stage height to serve as estimators of changes in river discharge.

In this regard, a high-magnitude flood is destructive and dangerous, making it difficult to collect these velocity and channel dimension measurements. Channel cross-sections are well known to experience significant changes during flood events (a common process is initial scouring and channel expansion during the rising phase of a flood wave, followed by filling during the waning phase; this leads to hysteresis in the stage-discharge relation). Most flood discharge estimates are thus based on rating curve extrapolations from lower energy conditions.

River flooding over a floodplain is an even more complicated phenomenon than in-channel discharge: a significant amount of the total flow may be occurring outside the main channel (Bjerklie et al., 2003). River water can flow over raised terraces, across multiple channels, and often outside of the measured cross-sectional domain —commonly defined by the river channel levees on floodplains. Once the levees are

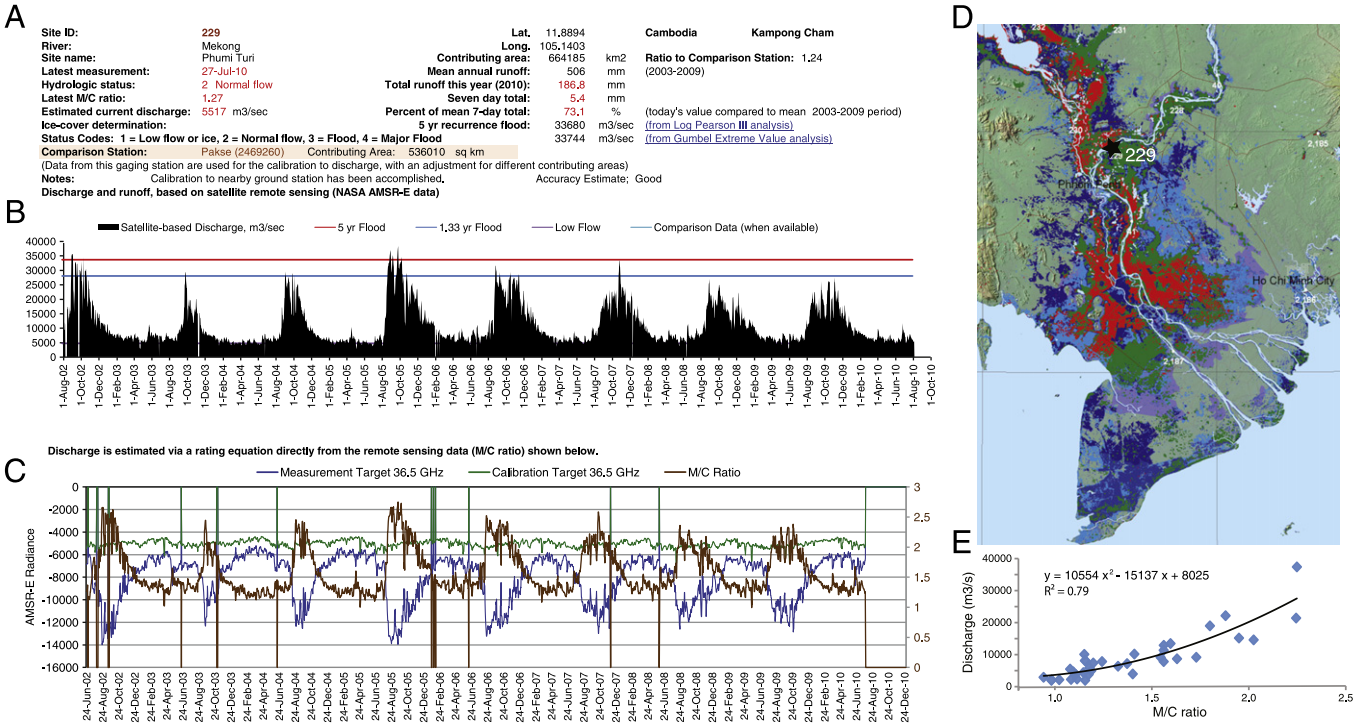

Fig. 11. Microwave-sensed river discharge (see text for details). A) DFO-River Watch station information (July 27, 2010) on Station 229, Mekong River, near the apex of the Mekong Delta. B) Daily discharge AMSRE estimates (2002–2010), in relation to the near annual and 5-y flood levels. C) Daily radiance measurement target of the river reach and a nearby calibration target (outside of the floodplain), with the resulting M/C ratio. D) Location map of the Mekong Delta showing the station location — colors indicate size of annual floods. E) Transformation of the remote sensing signal to actual discharge values on an international basis is accomplished by comparison of monthly means where at least intermittent gauging station data are available. The accuracy, and precision of such orbital measurements are tested along U.S. and European rivers with daily in situ discharge data.

Please cite this article as: Syvitski, J.P.M., et al., Floods, floodplains, delta plains — A satellite imaging approach, Sediment. Geol. (2012), doi:10.1016/j.sedgeo.2012.05.014

breached, the "missing" discharge must be estimated from inundation mapping on a daily basis, and this discharge must be added to channel discharge estimates. One of the few studies documenting these issues is from Sidorchuk (2003) who shows section-average velocity decreasing as stage height increases as the flood wave spreads across the floodplain.

To address some of these issues, we explore new methods to estimate discharge based on changes in flow width as sensed with scanning microwave radiometers, rather than the ground-based method of stage/flow depth discharge estimation. Fig. 11 provides one example of the standard data available for download from the DFO web site, for an AMSR-E station location on the Mekong River (site 229: Fig. 11D). River Watch offers more than 2500 global AMSR-E sites from which daily discharge estimates are made available since 2002. The AMSR-E research products continue to be refined (Syvitski and Brakenridge, submitted); they offer an eventual opportunity to accurately integrate flood inundation extent (as mapped by sensors such as MODIS) into long term flow series subject to exceedance probability analysis. Such new tools, analytical techniques and data, indicate that the quantification of global floodplain dynamics is within sight, and such work can be accomplished over each of the large-scale floodplain zones defined above.

7. Satellite data to improve floodplain models

Our answer to the question: "do our conceptual models of floodplain processes and architecture change in the era of global coverage of high-resolution remote-sensing data?" is affirmative for two reasons: the large spatial coverage and the detailed temporal coverage.

Remotely sensed topographic data (e.g. SRTM) does now systematically cover most lowland river floodplains at high spatial resolution. It allows sedimentary geologists unprecedented mapping of modern landscape and architectural characteristics. Future research should address the following questions:

- Do the large-scale distinct floodplain zones (container valley, floodplain depression, zones of nodal avulsion and fluvial delta plain) each have characteristic distributions of smaller-scale fluvial architectural elements?
- What is the subsurface expression of large-scale floodplain zones, and especially of tectonic depressions in a floodplain system?
- Can we identify necessary conditions for transitions between river patterns, by quantitatively classifying patterns over a variety of climatic regions, vegetation regimes and tectonic settings?

The high temporal resolution of satellite data provide us with an opportunity to better understand the processes of flooding of floodplains and collect flood measurements when direct observations are not possible or reliable, during times when much of the sediment transport and transitions in patterns occur. The MODIS and AMSR-E type-tools offer ways to sense high temporal resolution peak flood processes to address the following questions:

- How often and where are floodplains inundated, how does the flood extent relate to the active channel belt?
- Do large-scale distinct floodplain zones; container valley, floodplain depression, zones of nodal avulsion and fluvial delta plain, each have characteristic flooding behavior? How does this affect the floodplain deposition?
- At what peak flood conditions do levee breaks happen? Can we map crevasse splays after the floodwaters have waned?
- What are the different styles of flood-wave propagation over the full flooding period? Can these styles be related to flow strength and variation in flooding magnitude and frequency on the pattern?

8. Summary

This paper describes three orbital sensing data products for characterizing floodplains and their tendency for flooding: SRTM, MODIS and AMSR-E. The Space Shuttle SRTM survey provides geoscientists with quantitative data on the dimensions of the architectural elements and geomorphology of a global spectrum of floodplains. MODIS-based inundation mapping provides for the extent of global flooding during the last decade. AMSR-E offers a new method for estimating the daily discharge of floodplain-rivers that expand in width during flooding. Together this suite of data sources provides information into how landscapes develop across floodplains. The topographic resolution of the SRTM data is similar to the resolution of surfaces imaged with high quality 3D seismic surveys and this allows for direct comparison. Imaging of floodplain topography as a spatially continuous raster continues to improve in both horizontal (ASTER) and vertical (SAR, LIDAR) resolution.

Thirty-three floodplains and deltas are examined in terms of their large-scale floodplain landscape elements, and the location and size of floods within their floodplains over the last 10 years (Table 1). Smaller scale architectural elements include meander belts and associated scroll bars, braided river belts, anastomosing river channels, splay fans, channel levees, crevasse splay fingers, side entry fans, and the wide variety of floodplain lakes. These smaller features, sometimes with a vertical relief of not much more than a meter (e.g. crevasse splays leading off of a historical course of the Yellow River), were easily imaged and recognized in the topographical data. The character of abandoned channels can be measured and their sinuosity (among other descriptive statistics) compared to the modern channels. Differences might reflect climate changes or human engineering, or both.

Four main floodplain zones recognized are: container valleys, floodplain depressions, zones of nodal avulsions, and coastal deltas (Fig. 5). The container valleys are largely zones of sediment bypass, although many show a complex history of sediment aggradation with multiple levels of terracing: pulses of sediment may have moved through these systems. Avulsion zones are most common seaward of these container valleys. We have stressed the important role of floodplain depressions in reducing a river's transport of sediment downstream. Most depressions flood every year or two, helping to replenish both the water and sediment in the swamps and lakes covering their surface. The depressions often are zones of reduced down-valley slopes, with expanded widths and containing secondary overflow channels. Finally, the coastal deltas show many of the same features as floodplain depressions, with their lakes, multiple channels (at least historically), expanded widths and low downstream gradients. The ratio of the floodplain area to delta plain area ranged from 50:1 to 1: 30, a range much larger than anticipated. Nodal avulsions are also located at the landward side of coastal delta. Only a few continental-size rivers offer excellent examples of nodal avulsion within their oversized floodplains (e.g. Yellow, Indus, and Brahmaputra), but many more rivers showed evidence of nodal avulsion on their delta plains (e.g. Irrawaddy, Krishna).

We now have an excellent capability to map flood inundation on floodplains, globally and daily. The short record of measurement (one decade) hampers a full perspective to global flooding, which will be gained as flood observation and measurement continues over a longer period of time. In the meantime, statistical methods in combination with climate scenario numerical modeling might help to overcome the temporal limitations, and, given the increasingly appreciated "non-stationarity" of hydrologic time series in a period of climate and land use changes — the most recent past may be a more accurate indicator of present-day processes than longer term records. New methods in determining the daily discharge of rivers, globally, offer the potential to relate flood frequency and magnitude to the scale of floodwater inundation, and this in turn should allow the incomplete, commonly anecdotal, records of past "great floods" to be better examined and in the light of accurate maps of recent large floods. All of these techniques provide insight into how sediment and water are transported through floodplains and their delta plains. Finally, new techniques such as interferometric SAR-based subsidence mapping should allow large-scale areas of subsidence and their rates to be mapped, offering sedimentologists the prospect of combining surface process imaging and measurements of flooding and sediment

Please cite this article as: Syvitski, J.P.M., et al., Floods, floodplains, delta plains — A satellite imaging approach, Sediment. Geol. (2012), doi:10.1016/j.sedgeo.2012.05.014

transport to mapping of factors, such as subsidence, that may directly translate into preservation potential as a long term sedimentary deposit.

Acknowledgments

We thank NASA (NNXOTAF2SG/P207124; NNXOTAF28G/P207124), NSF (0621695), and ConocoPhillips for their financial support of this research. We also thank Albert Kettner for his technical support on this research.

References

Asselman, N.E.M., Middelkoop, H., 1995. Floodplain sedimentation, quantities, patterns and processes. Earth Surface Processes and Landforms 20, 481–499.
Berry, P.A.M., Garlick, J.D., Smith, R.G., 2007. Near-global validation of the SRTM DEM using satellite radar altimetry. Remote Sensing of Environment 106 (1), 17–27.
Bilham, R., Lodi, S., 2010. The Door Knockers of Mansurah,: Strong Shaking in a Region of Low Perceived Seismic Risk, Sindh, Pakistan. In: Sintubin, Manuel, Stewart, Iain S., Niemi, Tina M., Altunel, Erhan (Eds.), Special Paper 471 on Ancient earthquakes.
Bilham, R.S., Lodi, S., Hough, S. Bukhary, Khan, Abid Murtaza, Rafeeqi, S.F.A., 2007. Seismic hazard in Karachi, Pakistan: uncertain past, uncertain future. Seismological Research Letters 78 (6), 601–631.
Bjerklie, D.M., Dingman, S.L., Vorosmarty, C.J., Bolster, C.H., Congalton, R.G., 2003. Evaluating the potential for measuring river discharge from space. Journal of Hydrology 278, 17–38.
Blum, M.D., Törnqvist, T.E., 2000. Fluvial responses to climate and sea-level change: a review and look forward. Sedimentology 47 (Supplement 1), 2–48.
Brakenridge, G.R., 2010. , www.dartmouth.edu/~floods/AMSR-E%20Gaging%20Reaches/IndexMap.htm2010.
Brakenridge, R., Anderson, E., 2006. Modis-based Flood Detection, Mapping, and Measurement: the Potential for Operational Hydrologic Applications. Transboundary Floods: Reducing the Risks Through Flood Management: Nato science series: IV: earth and environmental sciences, 72, p. 1, http://dx.doi.org/10.1007/1-4020-4902-1_1. 1–12.
Brakenridge, G.R., Nghiem, S.V., 2004. Satellite-based flood detection, mapping, and river monitoring in near real time. Natural Hazards and Disaster Management Support Symposium, India-United States Conference on Space Science, Applications, and Commerce, Bangalore, India, p. 150.
Brakenridge, G.R., Tracy, B.T., Knox, J.C., 1998. Orbital remote sensing of a river flood wave. International Journal of Remote Sensing 19, 1439–1445.
Brakenridge, G.R., Nghiem, S.V., Anderson, E., Mic, R., 2007. Orbital Microwave Measurement of River Discharge and Ice Status. Water Resources Research 43, W0405, http://dx.doi.org/10.1029/2006WR005238 16 pp.
Bridge, J.S., 2003. Rivers and Floodplains: Forms, Processes, and Sedimentary Record. Wiley-Blackwell. 504 pp.
Chen, Z., Wang, Z., Finlayson, B., Chen, J., Yin, D., 2010. Implications of flow control by the Three Gorges Dam on sediment and channel dynamics of the middle Yangtze (Changjiang) River, China. Geology 38, 1043–1046.
Crutzen, P.J., Stoermer, E.F., 2000. The 'Anthropocene'. Global Change Newsletter 41, 17–18.
DeGroeve, T., Kugler, Z., Brakenridge, G.R., 2007. Near real time flood alerting for the global disaster alert and coordination system. In: de Walle, Van, Burghardt, P., Nieuwenhuis, C. (Eds.), Proceedings of the 4th International ISCRAM Conference. Delft, the Netherlands, May.
Edmonds, D.A., Hoyal, D.C.J.D., Sheets, B.A., Slingerland, R.L., 2009. Predicting delta 596 avulsions: implications for coastal wetland restoration. Geology 37, 759–762.
Erkens, G., 2009. Sediment Dynamics in the Rhine Catchment: Quantification of Fluvial Response to Climate Change and Human Impact. Netherlands Geographical Studies, 388. ISBN: 978-90-6809-431-2. 278 pp.
Farr, T.G., Rosen, P.A., Caro, E., Crippen, R., Duren, R., Hensley, S., Kobrick, M., Paller, M., Rodriguez, E., Roth, L., Seal, D., Shaffer, S., Shimada, J., Umland, J., Werner, M., Oskin, M., Burbank, D., Alsdorf, D., 2007. The Shuttle Radar Topography Mission. Reviews of Geophysics 45, RG2004, http://dx.doi.org/10.1029/2005RG000183.
Fenneman, N.M., 1906. Floodplains produced without floods. Geological Society of America Bulletin 38, 89–91.
Filizola, N., Fraizy, P., Guyot, J.L., Seyler, F., Baby, P., Herail, G., 2002. Actual Erosion by Rivers in the Bolivian Andes. Proceedings, 5th Intl. Symp. on the Andean Geodynamics: Toulouse, France, pp. 211–214.
Gallant, J.C., Read, A., 2009. Enhancing the SRTM Data for Australia. Proceedings of Geomorphometry 2009. Zurich, Switzerland, 31 August – 2 September, 2009, pp. 149–154.
Galloway, W.E., 1975. Process Framework for Describing the Morphologic and Stratigraphic Evolution of Deltaic Depositional Systems. In: Broussard, M.L. (Ed.), Deltas: Models for Exploration. Houston Geological Society, Houston, TX, pp. 87–98.
Galloway, W.E., Hobday, D.K., 1996. Terrigenous Clastic Depositional Systems. Springer, New York. 489 pp.
Hijma, M.P., 2009. From River Valley to Estuary — The Early-mid Holocene Transgression of the Rhine-Meuse Valley, The Netherlands. Netherlands Geographical Studies, 389978-90-6809-432-9. 192 pp.
Holmes, D.A., 1968. The recent history of the Indus. The Geographical Journal 134 (3), 367–382.
Hood, W.G., 2010. Delta distributary dynamics: extending, testing, and applying avulsion theory in a tidal system. Geomorphology, http://dx.doi.org/10.1016/j.geomorph.2010.07.007.
Kettner, A.J., Restrepo, J.D., Syvitski, J.P.M., 2010. A spatial simulation of fluvial sediment fluxes within an Andean drainage basin, the Magdalena River, Colombia. The Journal of Geology 118, 363–379.
Miall, A.D., 1996. The geology of fluvial deposits. Springer, New York. 582 pp.
Overeem, I. 2002. Process-response simulation of fluvio-deltaic stratigraphy. Delft University of Technology PhD thesis. ISBN 90 6464 859X.
Overeem, I., Syvitski, J.P.M., Hutton, E.W.H., 2005. Three-dimensional Numerical Modeling of Deltas. In: Giosan, L., Bhattacharya, J.P. (Eds.), River Deltas — Concepts, Models, and Examples. SEPM Special Publication No. 83, pp. 13–30.
Pizzuto, J., 1995. Sediment diffusion during overbank flows. Sedimentology 34, 301–317.
Postma, G., 1990. Depositional Architecture and Facies of River and Fan Deltas: A Synthesis. Special Publications International Association of Sedimentologists, 10, pp. 13–27.
Rowland, J.C., Dietrich, W.E., Day, G., Parker, G., 2009. Formation and maintenance of single-thread tie channels entering floodplain lakes: observations from three diverse river systems. Journal of Geophysical Research 114, F02013, http://dx.doi.org/10.1029/2008JF001073.
Schumann, G., Matgen, P., Cutler, M.E.J., Black, A., Hoffmann, L., Pfister, L., 2008. Comparison of remotely sensed water stages from LiDAR, topographic contours and SRTM. ISPRS Journal of Photogrammetry and Remote Sensing 63, 283–296.
Schumm, S.A., 1991. To Interpret the Earth: Ten Ways to be Wrong. Cambridge University Press, Cambridge UK. 131 pp.
Schumm, S.A., Brakenridge, G.R., 1987. River Responses. In: Ruddiman, W.F., Wright, H.E. (Eds.), North America and Adjacent Oceans During the Last Deglaciation: Geological Society of America, Decade of North American Geology, K-3, pp. 221–240.
Schumm, S.A., Dumont, J.F., Holbrook, J.M., 2002. Active Tectonics and Alluvial Rivers. Cambridge University Press, Cambridge UK. 276 pp.
Sidorchuk, A., 2003. Floodplain sedimentation: Inherited memories. Global and Planetary Change 39, 13–29.
Slingerland, R., Smith, N., 2004. River avulsions and their deposits. Annual Review of Earth and Planetary Sciences 32, 257–285.
Smith, K., Ward, R., 1998. Floods – Physical Processes and Human Impacts. John Wiley & Sons. 382 pp.
Stouthamer, E., Berendsen, H.J.A., 2007. Avulsion: the relative roles of autogenic and 633 allogenic processes. Sedimentary Geology 198, 309–325.
Syvitski, J.P.M., 2006. The morphodynamics of deltas and their distributary channels. In: Parker, G., Garcia, M. (Eds.), River, Coastal and Estuarine Morphodynamics. Taylor and Francis Group, London, pp. 143–160.
Syvitski, J.P.M., Saito, Y., 2007. Morphodynamics of deltas under the influence of humans. Global and Planetary Changes 57, 261–282.
Syvitski, J.P.M., Kettner, A.J., Correggiari, A., Nelson, B.W., 2005. Distributary channels and their impact on sediment dispersal. Marine Geology 222–223, 75–94.
Syvitski, J.P.M., Kettner, A.J., Hannon, M.T., Hutton, E.W.H., Overeem, I., Brakenridge, G.R., Day, J., Vörösmarty, C., Saito, Y., Giosan, L., Nicholls, R.J., 2009. Sinking deltas. Nature Geoscience 2, 681–689.
Vandenberghe, J., 2008. The fluvial cycle at cold–warm–cold transitions in lowland regions: a refinement of theory. Geomorphology 98, 275–284.
Walling, D., He, Q., 1997. Investigating spatial patterns of overbank sedimentation on river floodplains. Water, Air, and Soil Pollution 99, 9–20.
Wohl, E., 2007. Hydrology and Discharge. In: Gupta, A. (Ed.), Large Rivers: Geomorphology and Management. John Wiley & Sons, Ltd, West Sussex, pp. 29–44.
Zalasiewicz, J., et al., 2008. Are we now living in the Anthropocene? GSA Today 18, 4–8, http://dx.doi.org/10.1130/GSAT01802A.1.

Please cite this article as: Syvitski, J.P.M., et al., Floods, floodplains, delta plains — A satellite imaging approach, Sediment. Geol. (2012), doi:10.1016/j.sedgeo.2012.05.014